

## Assimilating Vortex Position with an Ensemble Kalman Filter

YONGSHENG CHEN AND CHRIS SNYDER

*National Center for Atmospheric Research,\* Boulder, Colorado*

(Manuscript received 14 July 2005, in final form 10 July 2006)

### ABSTRACT

Observations of hurricane position, which in practice might be available from satellite or radar imagery, can be easily assimilated with an ensemble Kalman filter (EnKF) given an operator that computes the position of the vortex in the background forecast. The simple linear updating scheme used in the EnKF is effective for small displacements of forecasted vortices from the true position; this situation is operationally relevant since hurricane position is often available frequently in time. When displacements of the forecasted vortices are comparable to the vortex size, non-Gaussian effects become significant and the EnKF's linear update begins to degrade. Simulations using a simple two-dimensional barotropic model demonstrate the potential of the technique and show that the track forecast initialized with the EnKF analysis is improved. The assimilation of observations of the vortex shape and intensity, along with position, extends the technique's effectiveness to larger displacements of the forecasted vortices than when assimilating position alone.

### 1. Introduction

Hurricane track forecasts have improved 1%–2% yr<sup>-1</sup> over the last 3 decades (Franklin et al. 2003). These improvements have followed from refinements of both numerical models and their initial conditions, the latter through improvements in satellite observations and their use, and through the addition of dropsondes from special reconnaissance flights (Burpee et al. 1996). The current National Hurricane Center's official track errors average 160 km for 24-h forecasts, increasing to 260 km at 48 h and 370 km at 72 h.

Despite the improvements in observations and data assimilation, initializing a realistic vortex in the correct location and with the correct storm motion remains a challenge. Many operational numerical weather prediction systems resort to vortex bogusing (Serrano and Undén 1994), though the analysis can be successful with a high-resolution model and sophisticated use of remotely sensed observations (Leidner et al. 2003). More-

over, hurricane forecast models, even the simplest 2D barotropic model, are highly nonlinear. Small initial errors in the vortex position, motion, and strength as well as the environmental flows may lead to large discrepancies in the short-term track and intensity forecast (Kurihara et al. 1993).

Ensemble forecasts, which acknowledge the initial uncertainties in the vortex and its environment, have also improved track forecasts (e.g., Zhang and Krishnamurti 1997, 1999; Cheung and Chan 1999a,b; Abernethy et al. 1998; Marchok et al. 2002; Weber 2003; Heming et al. 2004; Vigh 2004). When the uncertainties in the initial conditions and in the model physics are properly considered, the ensemble mean is, on average, closer to the real track than a single realization. In addition, the ensemble forecasts directly approximate strike probabilities. However, ensemble forecasts suffer similar difficulties in initializing the vortex.

Several methods exist to initialize a hurricane vortex in its correct position. Vortex bogusing techniques insert an initial vortex into a large-scale background field. The initial bogus vortex can be specified by combining empirical formulas or dynamical constraints with observations (e.g., Lord 1991; Serrano and Undén 1994; Leslie and Holland 1995; Krishnamurti et al. 1997; Davidson and Weber 2000; Zhu et al. 2002) or by transplanting a vortex with proper intensity and structure from a different simulation (e.g., Kurihara et al. 1993; Liu et al.

---

\* The National Center for Atmospheric Research is sponsored by the National Science Foundation.

---

*Corresponding author address:* Dr. Yongsheng Chen, NCAR, P.O. Box 3000, Boulder, CO 80307-3000.  
E-mail: yochen@ucar.edu

1997). Track prediction can be substantially improved if a vortex bogusging scheme generates a well-balanced initial vortex that induces fewer shocks in the forecast model (Bender et al. 1993; Kurihara et al. 1998). An alternative approach is to take simulated observations of surface pressure or low-level winds from a bogus vortex and assimilate them with a four-dimensional variational scheme using a large-scale background forecast (Zou and Xiao 2000; Xiao et al. 2000; Pu and Braun 2001). The structure of the resulting vortex is then determined in part by, and is potentially more consistent with, the dynamics of the assimilating model. The vortex relocation technique developed at the National Centers for Environmental Prediction (NCEP) relocates a misplaced hurricane vortex to the correct position in the background field prior to a three-dimensional variational (3DVAR) analysis. Liu et al. (2002) report improvements as large as 30% in hurricane track forecasts for both global and regional models at NCEP.

Another class of analysis schemes could also potentially be used to relocate a hurricane whose location was incorrect in the prior forecast. These share the idea that the analysis is a spatial distortion of the prior forecast, so that the analysis variables become a displacement field rather than the original state variables. Hoffman et al. (1995) used variational analysis to separate the distortion, amplification, and residual errors from the total forecast errors. Ravela et al. (2004) also applied variational methods to analyze a displacement field and align coherent structures. More recently, Lawson and Hansen (2005) proposed a new error model that includes a non-Gaussian alignment error and a Gaussian additive error, and they corrected two types of errors separately with an ensemble Kalman filter (EnKF).

These existing analysis techniques are meant to “move” the vortex a distance that is significant compared to the horizontal scale of the vortex. When the error of the forecast position is comparable to vortex scale, the forecast errors for model variables are likely to be significantly non-Gaussian, and linear assimilation schemes such as the EnKF may be far from optimal. In fact, hurricane position estimates routinely produced by the National Hurricane Center using satellite, radar, in situ aircraft, or synoptic observations are accurate relative to the size of vortex. These position estimates have errors of about 20 km for a mature hurricane (Elsberry 1995). Given that position observations are accurate and frequent, there seems to be no inherent reason that background forecasts should have large errors in vortex position. Linear assimilation

schemes are thus plausible approaches to the assimilation of hurricane position.

Using accurate and frequent position information, we will show in a 2D barotropic flow that a satisfactory ensemble analysis results from assimilating vortex positions with an EnKF and ignoring the non-Gaussianity of the forecast errors associated with finite displacements of the vortex. If the background forecast errors for vortex position are comparable to the vortex size, the linear EnKF update is noticeably suboptimal and produces artifacts such as double vortices for members whose positions are far from the mean. The barotropic experiments also demonstrate that assimilating additional information about the vortex, such as its shape or intensity, extends the range of displacements for which the EnKF is effective, although it does not resolve in any fundamental way the problems associated with a linear analysis scheme when background errors are non-Gaussian.

The plan of the paper is as follows: In section 2, we briefly review the EnKF. Section 3 gives a simple example of the EnKF update for an isolated vortex given observations of its position, shape, and intensity. Section 4 presents numerical results from a 2D barotropic model. The conclusions and discussion are summarized in section 5.

## 2. The ensemble Kalman filter

Atmospheric data assimilation is essentially a problem of estimating the state  $\mathbf{x}$  of the dynamical system (the atmosphere) from noisy observations  $\mathbf{y}$  taken on the state. From the Bayesian probability point of view, it is to obtain the conditional probability density function (pdf)  $p(\mathbf{x}_t|\mathbf{y}_t, \mathbf{y}_{1:t-1})$  of the state  $\mathbf{x}$  at time  $t$  given the observation  $\mathbf{y}_t$  taken at  $t$  and all previous observations  $\mathbf{y}_{1:t-1} = \{\mathbf{y}_1, \mathbf{y}_2, \dots, \mathbf{y}_{t-1}\}$ . The maximum likelihood estimate of the state  $\mathbf{x}_t$  is then the peak or mode of this pdf. When the pdf is symmetric and unimodal, the mode coincides with the conditional mean, and the maximum likelihood estimate is the same as the minimum variance estimate.

Bayes' rule states

$$p(\mathbf{x}_t|\mathbf{y}_t, \mathbf{y}_{1:t-1}) = \frac{p(\mathbf{y}_t|\mathbf{x}_t, \mathbf{y}_{1:t-1})p(\mathbf{x}_t|\mathbf{y}_{1:t-1})}{p(\mathbf{y}_t|\mathbf{y}_{1:t-1})}. \quad (1)$$

If the pdf of the present observation given the present state,  $p(\mathbf{y}_t|\mathbf{x}_t)$ , and the pdf of the state given previous observations,  $p(\mathbf{x}_t|\mathbf{y}_{1:t-1})$ , are known, the pdf of the state at the current time can be obtained easily given the assumption that the observations at different times are conditionally independent given the state. The Bayesian probabilistic estimation approach is theoretic-

cally appealing but practically infeasible for real atmospheric problems because of the computational cost.

Under the assumptions of Gaussian error statistics, linear dynamics, and observation operators, the Kalman filter (Kalman 1960; Kalman and Bucy 1961) is equivalent to the Bayesian approach. The Kalman filter recursively updates the state and its error covariance using new observations and then propagates the state forward until new observations are available. The Kalman filter requires less computation than a fully Bayesian approach, but its cost is still prohibitive for high-dimensional systems.

The EnKF provides a generalization and computationally feasible approximation of the Kalman filter update. It was first applied in oceanography by Evensen (1994) and in atmospheric science by Houtekamer and Mitchell (1998). Since then, many studies have been conducted to advance this technique. A recent overview of the EnKF can be found in Evensen (2003). The EnKF has shown potential for data assimilation in the atmosphere at both large scales (Houtekamer and Mitchell 1998; Hamill and Snyder 2000; Whitaker and Hamill 2002; Mitchell et al. 2002; Anderson et al. 2005; Houtekamer et al. 2005) and mesoscales (Snyder and Zhang 2003; Zhang et al. 2004; Dowell et al. 2004).

Suppose the observations are related to the state by  $\mathbf{y} = \mathbf{H}\mathbf{x} + \boldsymbol{\epsilon}$ , where  $\mathbf{H}$  is the linear observation operator and  $\boldsymbol{\epsilon}$  is a Gaussian random variable with mean zero and covariance  $\mathbf{R}$ . Then the update equations of the Kalman filter (at time  $t$ ) are

$$\bar{\mathbf{x}}^a = \bar{\mathbf{x}}^f + \mathbf{K}(\mathbf{y}^o - \mathbf{H}\bar{\mathbf{x}}^f), \quad (2a)$$

$$\mathbf{K} = \mathbf{P}^f \mathbf{H}^T (\mathbf{H} \mathbf{P}^f \mathbf{H}^T + \mathbf{R})^{-1}, \quad \text{and} \quad (2b)$$

$$\mathbf{P}^a = (\mathbf{I} - \mathbf{K}\mathbf{H})\mathbf{P}^f. \quad (2c)$$

Here,  $\mathbf{y}^o$  is a specific realization of the observations, the overbar denotes the mean of the state vector  $\mathbf{x}$ , and  $\mathbf{P}$  is its covariance matrix. The superscripts  $f$  and  $a$  indicate, respectively, forecast (or background) quantities conditioned on the knowledge of observations prior to time  $t$  and analysis quantities conditioned on all observations including  $\mathbf{y}^o$ .

In the EnKF, the analysis equation for the ensemble mean has the same form as (2), but  $\mathbf{P}^f \mathbf{H}^T = \text{cov}(\mathbf{x}^f, \mathbf{H}\mathbf{x}^f)$  and  $\mathbf{H}\mathbf{P}^f \mathbf{H}^T = \text{cov}(\mathbf{H}\mathbf{x}^f, \mathbf{H}\mathbf{x}^f)$  are approximated using sample covariances from the ensemble of model forecasts (Evensen 1994). These sample covariances can also be computed for nonlinear observation operators,  $H(\mathbf{x})$ . For example, using the subscript  $i$  for ensemble members,  $\text{cov}[\mathbf{x}_i^f, H(\mathbf{x}_i^f)]$  can be approximated by the sample covariance

$$\frac{1}{N_e - 1} \sum_{i=1}^{N_e} (\mathbf{x}_i^f - \bar{\mathbf{x}}^f) [H(\mathbf{x}_i^f) - \overline{H(\mathbf{x}^f)}],$$

where  $N_e$  is the number of ensemble members and, in a slight abuse of notation, overbars now denote an ensemble average.

The EnKF also updates the deviation from the mean of each member as a counterpart to (2a). We use an ensemble square root filter following Whitaker and Hamill (2002) and assimilate observations serially. The update equation for the deviation of the  $i$ th member from the mean is

$$\mathbf{x}_i^a - \bar{\mathbf{x}}^a = \mathbf{x}_i^f - \bar{\mathbf{x}}^f - \alpha \mathbf{K} [H(\mathbf{x}_i^f) - \overline{H(\mathbf{x}^f)}]. \quad (3)$$

The factor  $\alpha$  is included in (3) so that the sample covariance of  $\mathbf{x}^a$  approaches that given by (2c) as  $N_e$  increases. For an individual observation with a standard deviation of  $\sigma_o$ , Whitaker and Hamill (2002) show

$$\alpha = \left\{ 1 + \sqrt{\frac{\sigma_o^2}{\text{var}[H(\mathbf{x}^f)] + \sigma_o^2}} \right\}^{-1}, \quad (4)$$

where  $\text{var}[H(\mathbf{x}^f)]$  is again computed as a sample variance. Although such refinements are not required in the present work, correlated observation errors can be handled either by considering linear combinations of the observations that are statistically uncorrelated or by processing correlated observations in batches, which involves inverting small matrices instead of scalars as in the one-at-a-time serial update.

After the above update procedure, the ensemble members are forecast forward in time using the full model until new observations are available. This is a Monte Carlo approximation to the propagation in time of the state's pdf. Though model errors can be considered in this step, we consider only perfect forecast models in this study.

### 3. A simple example

This section illustrates the spatial structure of corrections to a vortex given observations of its position. We also discuss problems in the EnKF update that arise when the uncertainty in the position is comparable to the vortex scale and how assimilating observations of the vortex intensity or shape can partially ameliorate those problems. We consider the EnKF update for an idealized 2D axisymmetric vortex given a single position observation and a prior ensemble whose members have the correct vortex structure but incorrect locations.

#### a. Assimilating position

The system state is defined by the vorticity  $\zeta$  on  $256 \times 256$  equally spaced grid points covering a  $2400 \text{ km} \times 2400 \text{ km}$  domain. We take the true vortex to have

an axisymmetric Gaussian vorticity profile with a maximum value of  $5 \times 10^{-4} \text{ s}^{-1}$  at the center and a decay scale of 80 km in the radial direction. We assume that each of the 30 members of the prior or “forecast” ensemble has the same vortex profile as the true vortex and that each member’s vortex, as well as the true vortex, has center coordinates that are drawn randomly from a Gaussian distribution with a mean equal to the domain midpoint (1200 km, 1200 km) and variance  $\sigma_f^2$ .

The vortex center position is determined from the vorticity field  $\zeta$  through the observation operator  $H$ , which is defined as an algorithm to find the vorticity-weighted center. Specifically, the algorithm first finds the grid point with maximum vorticity and defines a small box ( $9 \times 9$  grid points) centered at that grid point. (For vorticity fields with multiple maxima, the box is centered on the global maximum.) The algorithm then returns the vorticity-weighted average over the box of each coordinate ( $x$  and  $y$ ) as the vortex center coordinates. The observation of the center position for the true vortex is also contaminated by independent Gaussian random errors in both the  $x$  and  $y$  components with mean zero and variance  $\sigma_o^2$ . In this paper, we assume  $\sigma_o = 20$  km.

Figure 1 depicts the change of vortex position from each member after assimilating the position observation, along with the ensemble mean vorticity increment. Two cases are shown: initial position errors smaller than the vortex radius ( $\sigma_f = 20$  km; Figs. 1a,b) and comparable to the vortex radius ( $\sigma_f = 80$  km; Figs. 1c,d).

When the initial position errors are small, the analysis corrects the member vortices’ positions toward the observed center (Fig. 1a). The ensemble mean of the analysis positions is approximately the average of the observed and prior mean positions (each weighted according to the other’s error variance), and the ensemble spread of position shrinks from prior to analysis. The analysis update imposes on the ensemble mean (and each member’s) vorticity field a dipole of vorticity increments, which shifts the vortex toward the observed position. The maximum magnitude of the increments for the ensemble mean is 1 order smaller than the maximum vorticity of the ensemble mean vortex.

To understand why the EnKF produces the update shown in Fig. 1b, consider the prior statistics on  $\zeta$ . Since the member vortices differ only by a small Gaussian displacement  $(\delta x, \delta y)$  with variance  $\sigma_f^2$  in each coordinate, the vorticity of a member vortex at any grid point  $(x_i, y_j)$  can be written as

$$\begin{aligned} \zeta(x_i, y_j) &= \zeta_0(x_i - \delta x, y_j - \delta y) \\ &= \zeta_0(x_i, y_j) - (\delta x, \delta y) \cdot \nabla \zeta_0 + O(\delta x^2, \delta y^2), \end{aligned} \quad (5)$$

where  $\zeta_0(x, y)$  is the vorticity of the “reference” vortex from which each member is derived. When  $|(\delta x, \delta y)|$  is sufficiently small, the higher-order nonlinear terms can be ignored. The vector of gridpoint vorticities is then approximately Gaussian,

$$\boldsymbol{\zeta} \sim N(\boldsymbol{\zeta}_0, \sigma_f^2 \mathbf{G}\mathbf{G}^T),$$

where  $\mathbf{G}$  has two columns that contain gridpoint values of  $\partial \zeta_0 / \partial x$  and  $\partial \zeta_0 / \partial y$ , respectively. Lawson and Hansen (2005, their appendix A) derive a similar result in one spatial dimension. The EnKF therefore gives an optimal update on vorticity in the limit that  $(\delta x, \delta y)$  is small.

The spatial structure of the EnKF update is determined by

$$\text{cov}[\zeta(x_i, y_j), (\delta x, \delta y)] = -\sigma_f^2 \nabla \zeta_0,$$

again neglecting terms in (5) that are nonlinear in  $\delta x$  and  $\delta y$ . This covariance, when dotted with the difference between the observed and ensemble mean positions, gives an increment in the form of a dipole aligned in the direction of the difference, as shown in Fig. 1b.

When displacements are comparable to the vortex radius, the higher-order terms in (5) cannot be omitted, and the vorticity becomes non-Gaussian even though the displacement is Gaussian. Thus, the EnKF update, which depends only on the mean and the covariance of the ensemble, may be far from optimal. As an example, the EnKF update for initial position errors with  $\sigma_f = 80$  km is shown in Figs. 1c,d. The magnitude of the vorticity increments for the ensemble mean now become comparable to the vortex itself, and non-Gaussian effects appear. In particular, the spread of positions increases in the analysis and the ensemble mean position does not fit the observation, despite the fact that  $\sigma_o = \sigma_f/4$ . The EnKF update is clearly suboptimal for the vortex position.

As in the case with  $\sigma_f = 20$  km, the mean vorticity increment (Fig. 1d) is a dipole and acts to shift the ensemble mean vortex toward the observed position. (The increment does, however, have a larger spatial scale when the displacements are larger—note that Figs. 1b,d display domains of different sizes.) The suboptimality of the position update comes from problems in the vortex structure of individual members, which lead to the position of the mean vortex after the analysis differing from the mean position of the updated members.

Figure 2 shows two members before and after the update. Member 3 has small initial displacement from the center of the mean vortex and its center position is correctly shifted toward the observation with little dis-

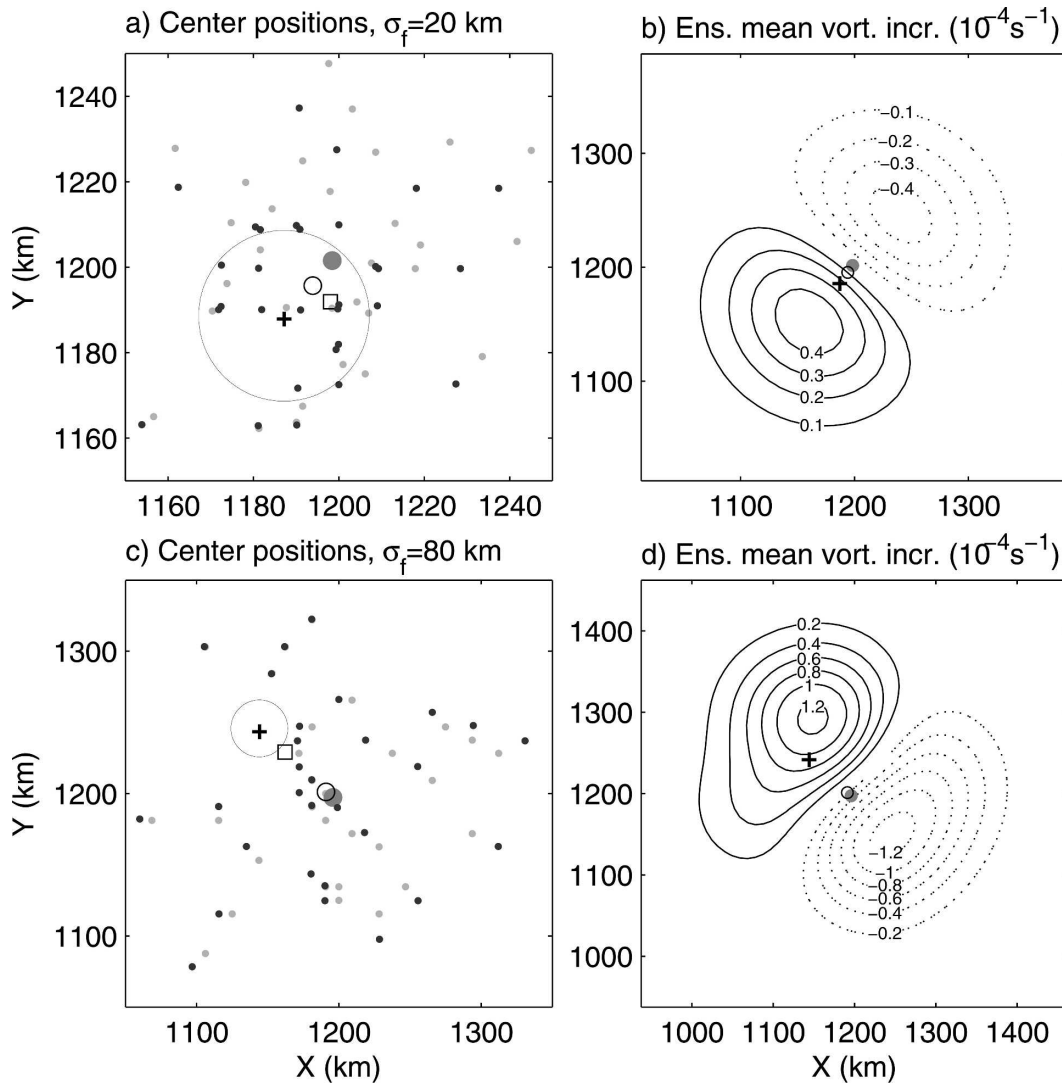


FIG. 1. EnKF update for initial position errors of (a),(b)  $\sigma_f = 20$  km and (c), (d)  $\sigma_f = 80$  km. In (a), (c), it is shown how the vortex center position changes. The prior and posterior center positions of 30 ensemble members are denoted by gray and black dots, with their mean positions labeled by a large gray dot and a small circle, respectively. The true center position is marked by a square and the observed position by a cross. The big circle is centered at the observation and has a radius of 20 km to represent the observational error. In (b), (d), the vorticity increments ( $\times 10^{-4} \text{ s}^{-1}$ ) for the ensemble mean vortices are plotted. Negative values are in dotted contours and zero contours are omitted. The ensemble mean positions of the forecast, the analysis, and the observation are plotted as a gray dot, a circle, and a cross, respectively. Note that domain sizes are different in (a)–(d).

ruption of the vortex structure. Member 10, however, has a larger initial displacement and becomes a binary vortex in the analysis, with a secondary vortex added near the observed center. To see why this occurs, consider member 10's vorticity increment in the EnKF analysis. The increment depends, through the gain  $\mathbf{K}$ , on  $\text{cov}[\zeta(x_i, y_j), (\delta x, \delta y)]$  and thus has a dipolar structure like that in Fig. 1d (though with different orientation). Member 10's vortex is displaced sufficiently far that it lies almost entirely within the negative lobe of

the dipole. The increment then weakens the original vortex and produces a new, separate vortex under the positive lobe.

It remains to be seen whether these pathologies in the EnKF update will grow worse with repeated assimilation of position through multiple assimilation cycles. We will turn to this question, among others, in section 4. Since vortex structure and intensity can be corrupted when displacements are not small, there is also the possibility that additional observations can compensate at

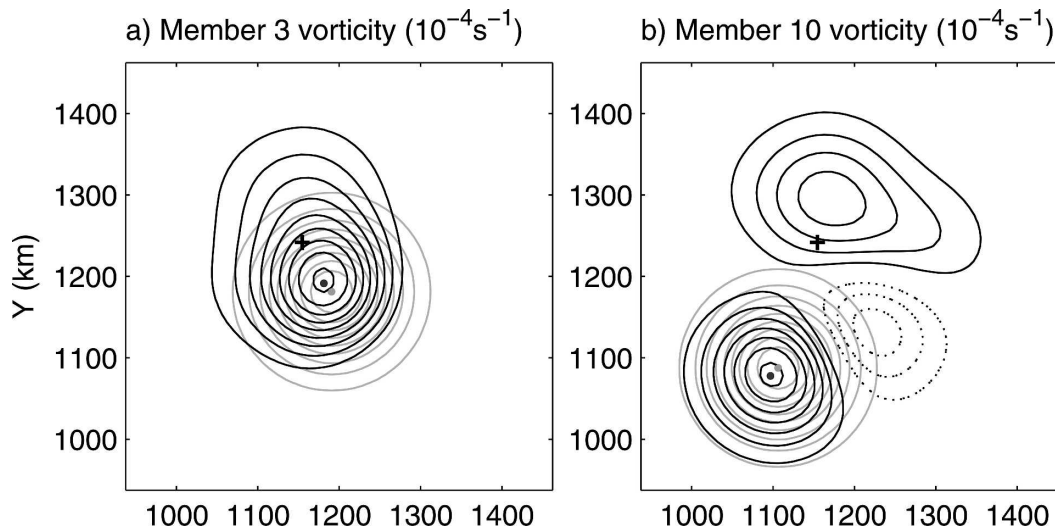


FIG. 2. Prior (gray contours) and posterior (black contours) vorticities of members (a) 3 and (b) 10 for initial position errors of  $\sigma_f = 80$  km. The contours have intervals of  $0.5 \times 10^{-4} \text{ s}^{-1}$  with zero contours omitted and negative values dotted. The gray dot, the black dot, and the cross denote the prior, posterior, and observed centers, respectively.

least partially for the pathologies of the position assimilation. This issue is considered next.

#### b. Assimilating shape and intensity

Satellites and radars cannot only define the position of a hurricane, but also provide information about its shape and intensity. For example, hurricane intensity is routinely estimated using the Dvorak technique, which utilizes satellite imagery (Dvorak 1975, 1984). Accurate shape and intensity observations, like position observations, may be valuable for data assimilation.

The experiments here and in section 4 use shape and intensity observations that are formulated as follows: The simplest and arguably most physically relevant model for a nonaxisymmetric vortex is the elliptical vortex. We assume that we are given observations of the length of the vortex's major and minor axes and its rotation angle from the  $x$  axis. These three shape parameters are determined by fitting an ellipse to the isoline of the half value of the maximum vorticity using the elliptic Fourier descriptor method (Kuhl and Giardina 1982) as described in the appendix. The observational errors for the shape parameters are assumed to be Gaussian with standard deviations of 20 km for the major and minor axes and  $45^\circ$  for the rotation angle. For intensity, we take the observations to be defined by the sum of the vorticity inside the same  $9 \times 9$  box of grid points surrounding the location of maximum vorticity that was used in determining the vortex center. The observational error for the intensity is Gaussian with mean 0 and variance  $10^{-6} \text{ s}^{-2}$ , which is 1 order of

magnitude smaller than the intensity itself. For both types of observations, the same observation operator is used in simulating the observations and for the assimilation.

The 20-km standard deviation of observation error in the major and minor axes means that observations of the major axis are frequently smaller than observations of the minor axis. In the experiments in both this section and the next, it matters little whether the major-axis observation is always identified correctly with the major axis of the simulated vortices or simply taken to correspond to the largest of the two axis observations.

When the vortex shape and intensity are uncertain in the prior forecast, optimal assimilation of these observations will of course improve the analysis. The small uncertainty limit for either shape or intensity can be analyzed in a manner analogous to that given in the previous subsection for position observations: the pdf for vorticity is approximately Gaussian when the shape or intensity uncertainty is small and the EnKF update approximates the optimal analysis to within sampling error. We will not consider the case of small uncertainty further here.

Assimilation of shape or intensity observations can also have another role. By bringing additional information to the analysis, these observations can help correct problems in the EnKF assimilation of position that occur when displacements of the forecast vortices are not small.

We illustrate this second role with two examples. Both begin with a prior ensemble in which, as in the

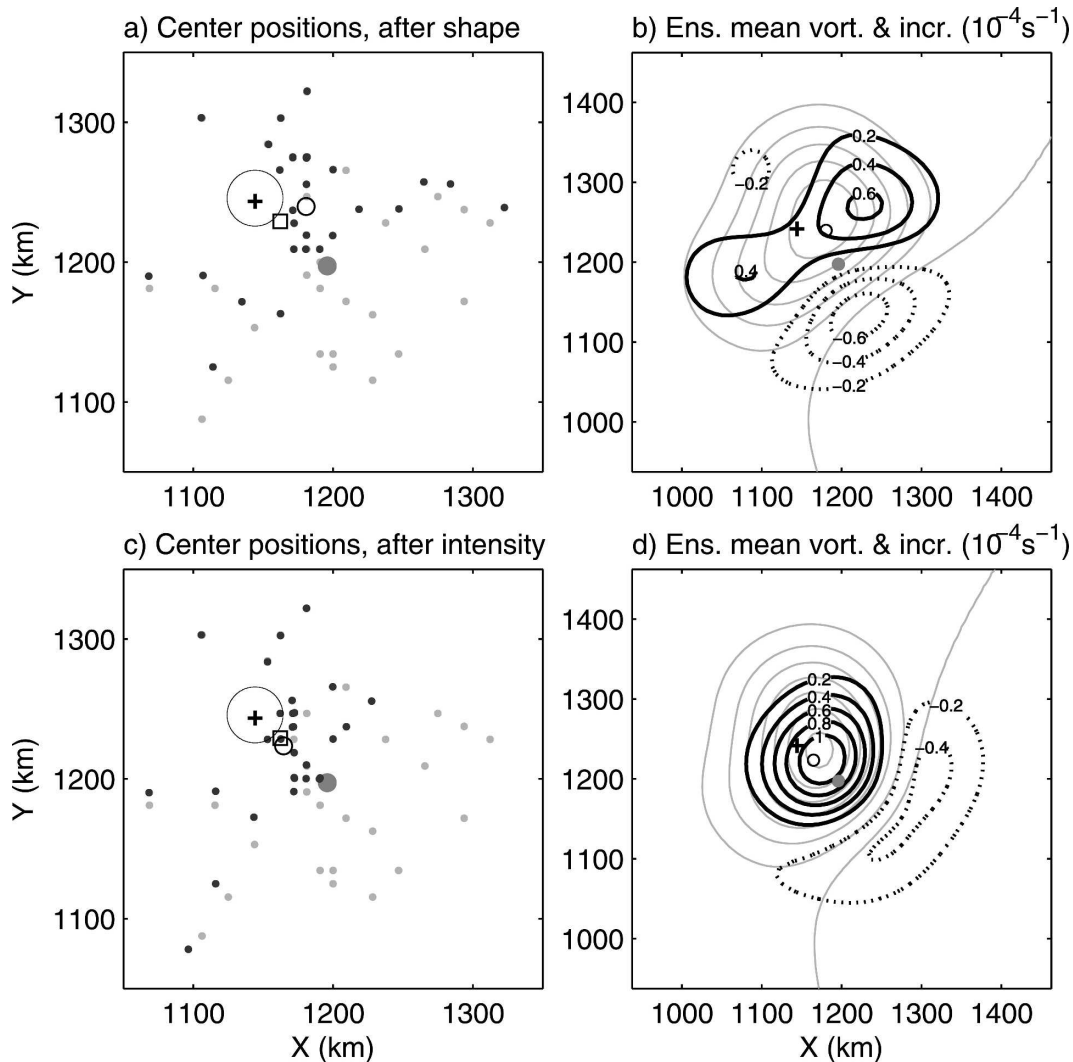


FIG. 3. Same as Fig. 1, but for the center position changes and the vorticity increments after sequentially assimilating the (a), (b) shape or (c), (d) intensity following the assimilation of the position showing in Figs. 1c,d. The vorticity increments are relative to the vorticity fields, which have been updated by assimilating the position. The posterior ensemble mean vorticity is plotted in gray contours (with intervals of  $0.5 \times 10^{-4} \text{ s}^{-1}$ ) in (b) and (d).

previous subsection, each member has a vortex with identical structure but different locations whose spread of 80 km is comparable to the vortex radius. After updating this ensemble given an observation of the vortex position, we then assimilate either shape or intensity observations. Before assimilating position, the shape of each member's vortex is the same, as is its intensity. The covariance of the shape parameters or intensity with vorticity is therefore zero and so is the gain  $\mathbf{K}$  for either shape or intensity observations. Thus, it is crucial in both examples that position is assimilated first.

The EnKF update based on the shape observations is shown in Figs. 3a,b. For the sake of clarity, the same ensemble members and position observation as in Fig.

1c are used. Assimilating the shape parameters improves the positions of the members' vortices and reduces the spread of positions.

To see how the improvements come about, recall that the dipolar vorticity increments from the position assimilation can distort a member's vortex or add a secondary vortex. These distortions are an artifact of the suboptimal position update for displacements comparable to the vortex radius. They tend to be aligned with the direction of the displacement and produce substantial variability in the major and minor axes (standard deviations of 32 and 15 km, respectively, in this example). The mean increment (Fig. 3b) reflects these distortions. Vortices on average contract along the di-

rection of the mean displacement from the observed position and lengthen in the orthogonal direction. The vortex position then tends to move (or possibly jump, when a secondary vortex is present) toward the observed position.

Figures 3c,d display the EnKF update given an observation of vortex intensity, again following assimilation of position. Just as with shape observations, assimilation of vortex intensity improves the position of the member vortices. The update in this case relies on covariances of vorticity and intensity, which appear because the position assimilation weakens vortices more the farther they lie from the mean position (see Fig. 2). The resulting mean vorticity increment amplifies the vorticity in regions between the prior mean center and the observed center and further weakens vortices far from the observed center.

We emphasize that assimilating shape and intensity does not eliminate the problems that appear in the EnKF assimilation of position when displacements are comparable to the vortex radius and vorticity errors are not approximately Gaussian. Although Fig. 3 indicates that members' vortex positions and the mean vortex are improved, many members still exhibit the double vortices or severely distorted vortex structure produced by the EnKF assimilation of position. It remains to be tested whether the changes produced by assimilating shape or intensity will be helpful in a cycling assimilation system. We address this question in the next section.

#### 4. Experiments with a barotropic model

##### a. Model and experiment design

In this section, we investigate the assimilation of the vortex position, shape, and intensity information with an EnKF in the context of a simple barotropic nondivergent model. This model clearly lacks many of the processes that influence the track and the evolution of real hurricanes, including the planetary boundary layer, vertical shear of the environmental wind, and latent heat release. At the same time, similar models have been used for operational forecasting of hurricane tracks. For example, the 2D nested barotropic model VICBAR provides valuable operational guidance to the hurricane forecast at the National Hurricane Center (DeMaria et al. 1992; Aberson and DeMaria 1994). Barotropic models can capture the key dynamics that affect hurricane tracks, namely the steering by and interaction with the environmental flow. Simplicity and cheap computations make the barotropic model a useful vehicle for the first test of assimilation of hurricane

position, shape, and intensity, prior to more complex and costly experiments with mesoscale models.

The model equation is

$$\frac{\partial \zeta}{\partial t} + \frac{\partial(\psi, \zeta)}{\partial(x, y)} = \nu \nabla^4 \zeta, \quad (6)$$

where  $\psi$  is the streamfunction,  $\zeta = \nabla^2 \psi$  the vorticity, and  $\partial(\cdot, \cdot)/\partial(x, y)$  the Jacobian operator. The model is cast on a 2400 km  $\times$  2400 km, doubly periodic Cartesian domain with 256  $\times$  256 equally spaced grid points. Time differencing is accomplished with a fourth-order Runge–Kutta scheme and the time step is 60 s. The nonlinear term in (6) is calculated pseudospectrally and includes the application of the “two-thirds” alias-free rule. A fourth-order hyperdiffusion inhibits the accumulation of enstrophy at the smallest resolved scales.

The model was initialized with a random vorticity field containing only wavenumbers 2–10. After a 240-h integration, the flow is dominated by coherent vortices, which are surrounded by weak filaments that decay through the fourth-order dissipation (cf. Fig. 4a). This vorticity field (with maximum absolute value of roughly  $10^{-4} \text{ s}^{-1}$ ) will be taken as the ensemble mean large-scale environmental flow in the subsequent experiments.

In these subsequent experiments, we assume for simplicity that the initial vortex structure is known, but its position and the environmental flow are uncertain. An initial ensemble of 31 members is therefore constructed as follows: The environmental vorticity field is perturbed by random errors in wavenumbers 2–10 with maximum amplitude of  $10^{-5} \text{ s}^{-1}$ . A vortex with identical structure but varying location is added to each perturbed environmental flow, following the procedure outlined in section 3a. We then take the first of the states to be the initial conditions for the reference, or truth, simulation and the other 30 states as the initial conditions for ensemble members.

All of the results in what follows are subject to some random variability owing to the specific realization of both the initial ensemble and the observation errors. We have performed multiple realizations of most of the experiments. Except where noted, none of our results change qualitatively under different realizations of the ensemble and observation errors.

For later reference, Table 1 summarizes the settings for all of the experiments.

##### b. Ensemble track divergence

The first experiment, EXPERR, illustrates the error growth in the ensemble prediction. Thirty members are used along with the reference, or truth, simulation from

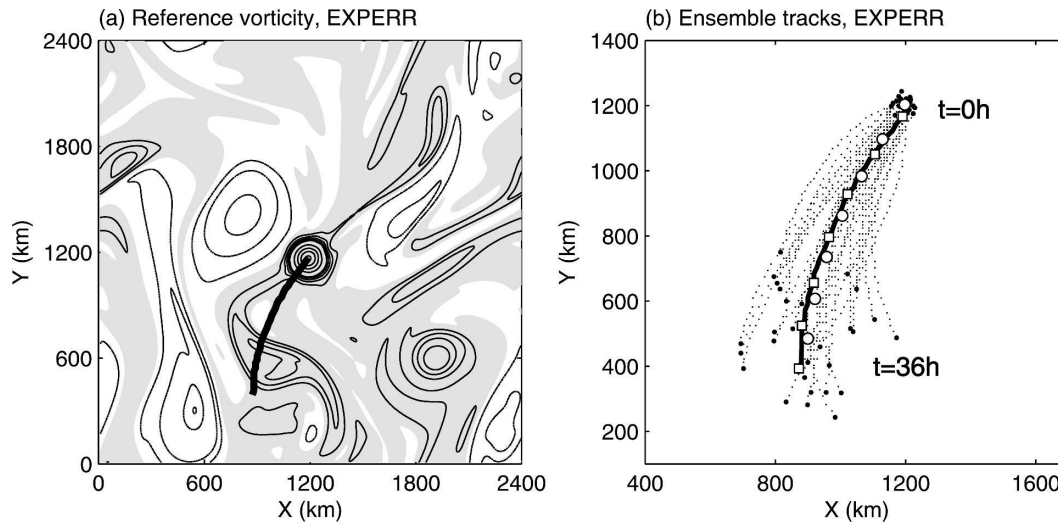


FIG. 4. (a) The initial vorticity field of the reference simulation, in units of  $10^{-4} \text{ s}^{-1}$  and contoured at  $\pm 0.2$ ,  $\pm 0.4$ ,  $\pm 0.6$ ,  $\pm 0.8$ ,  $\pm 1$ , 2, 3, 4, and 5. Positive regions are shaded. The thick solid line denotes the track of the center in 36 h. (b) The ensemble tracks in EXPERR, shown on a smaller domain than (a). The thick solid line is the same reference track as in (a) with squares indicating 6-h positions. The 1-h center positions of 30 ensemble members are marked by the small dots (highlighted by larger dots at 0 and 36 h). The 6-h ensemble mean center positions are shown by the circles.

which observations will be taken. The initial Gaussian position error has a standard deviation of  $\sigma_f = 20 \text{ km}$ .

All of the members and the reference are integrated forward for 36 h. Figure 4 plots the initial vorticity field of the reference simulation and the tracks for the reference vortex and all the members as well as their mean. The tracks start to diverge from the beginning. The position spread among the ensemble members is about 91 km at 24 h and 127 km at 36 h. The ensemble mean track is slower than the reference simulation even though they align closely by chance in this realization.

### c. Assimilating position with EnKF

The next experiments explore the effect of assimilating vortex position. Observations of the vortex charac-

teristics are constructed by adding random observational errors to the values taken directly from the reference simulation. The center position observations are the exact positions  $(x, y)$  plus independent Gaussian random errors of zero mean and variance  $\sigma_o^2 = 20^2 \text{ km}^2$ .

In experiment EXPR20, the reference and the ensemble members are initialized as in EXPERR, but the position observations are assimilated into the model every hour beginning at 1 h and continuing to 24 h. Figure 5 shows the ensemble tracks and the track errors. Comparing with EXPERR, the ensemble tracks have been corrected toward the real track. Figure 5b indicates that the ensemble spread decreases to 13 km over the first two assimilation cycles. Even though the 1-h forecast following the analysis tends to increase the

TABLE 1. Summary of the experiments. The initial position errors and the observational errors are assumed to be Gaussian. The std devs of the observational errors are shown in the second column when they are assimilated. In all experiments with assimilation, observations are available and assimilated every hour.

Expt	Assimilating			Std dev of initial position error (km)	Assimilation window (h)
	Position	Shape	Intensity		
EXPERR	No	No	No	20	No
EXPR20	20 km	No	No	20	1–24
EXPR20I	20 km	No	$10^{-3} \text{ s}^{-1}$	20	1–24
EXPR80	20 km	No	No	80	1–24
EXPR80S	20 km	20 km, $45^\circ$	No	80	1–24
EXPR80I	20 km	No	$10^{-3} \text{ s}^{-1}$	80	1–24
EXPR80IS	20 km	20 km, $45^\circ$	$10^{-2} \text{ s}^{-1}$	80	1–24
EXPF	No	No	No	20	No
EXPR80ISF	20 km	20 km, $45^\circ$	$10^{-2} \text{ s}^{-1}$	80	1–12

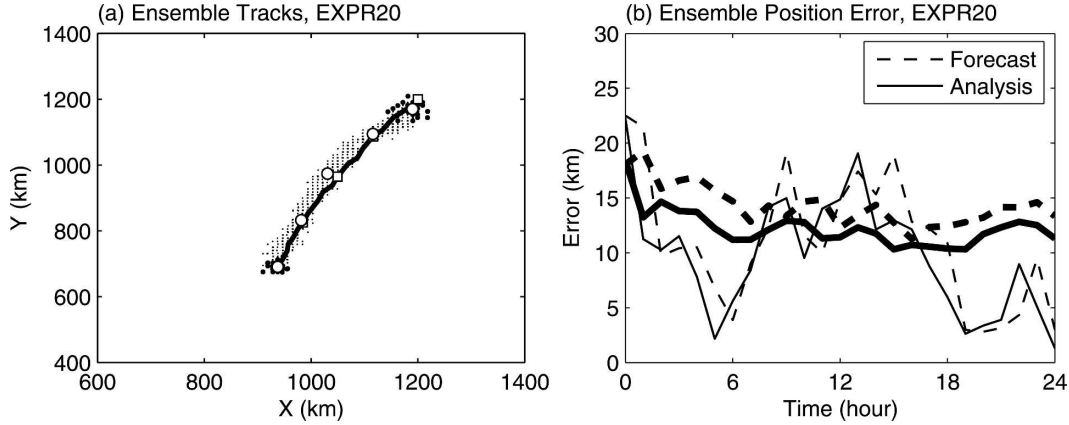


FIG. 5. Tracks and track errors in EXP20. (a) Same as Fig. 4b, but the positions are at the update steps and only for a period of 24 h. The  $x$  axis is enlarged to show the tracks clearly. (b) The time evolution of the position errors of the ensemble mean (thin lines) and the ensemble spread for vortex position (thick lines). The dashed and solid lines denote the values at the forecast steps (prior) and the update steps (posterior), respectively.

spread again, the periodic assimilation keeps the spread at roughly 12 km.

The error of the ensemble mean track after the analysis, on the other hand, is more variable, though it remains less than 20 km throughout the experiment (Fig. 5b). Here the track error is defined as the root-mean-square error (rmse) of the center coordinates ( $x$ ,  $y$ ) from the *true* center positions in the reference simulation rather than from the observations. The observational errors sometimes push the ensemble mean analysis away from the truth, as may happen to any data assimilation scheme with imperfect observations (Morss et al. 2001).

Experiment EXP20 shows that our assimilation technique produces a satisfactory analysis. This is not only because the EnKF update is nearly optimal when the prior position errors are small but also because of the internal dynamics of the vortex itself. Studies have shown that smoothly distributed and rapidly rotating vortices can quickly axisymmetrize weak anomalies (Melander et al. 1987; Carr and Williams 1989; Sutyrin 1989; Smith and Montgomery 1995), such as might be produced by the EnKF update for small position errors.

When the forecast displacement is sufficiently large, however, the EnKF analysis can severely distort the vortex in each member, as was shown in Fig. 2b. Dynamical effects alone then may not be enough to recover a more symmetric vortex at later times. Large displacements can happen when, for example, a tropical cyclone has no clearly defined eye and the observational error of the center location is large or when observations are so infrequent that the forecast errors for the vortex position are large. The performance of the EnKF under large initial displacements is examined next.

In experiment EXP80, the initial positions of the vortices in 30 ensemble members and in the reference are randomly perturbed by Gaussian errors of mean zero and variance  $\sigma_f^2 = 80^2 \text{ km}^2$ . The rest of the settings are the same as in EXP20. The ensemble tracks shown in Fig. 6 have a larger spread than EXP20 (cf. Fig. 5). The spread increases to about 100 km during the first 15 h before it starts to decrease.

As discussed in section 3, some members' vortices are likely to have been substantially distorted by the EnKF update, but Fig. 6 tells nothing about that aspect. We now define a correlation diagnostic that quantifies the degree of distortion in the vortex structures. To compare only the structural differences of the vortices regardless of their positions, a small area ( $21 \times 21$  grid points) is chosen for each member or the true state surrounding its own vortex center, and the correlation between each member's vorticity in these small areas and that of the true state is computed. Figure 7 plots the distribution of the ensemble correlations and its mean value at each of the forecast and update steps. The ensemble mean correlation decreases with time to below 0.8 at 24 h. This is a symptom of the same "binary vortex" problem discussed in section 3.

To emphasize problems arising when displacements of vortices are large, we have shown the worst case among several realizations of EXP80. In some realizations, the track spread decreases gradually to a steady value of about 20 km in a few hours, and each member's vortex gradually returns to an approximately axisymmetric structure.

#### d. Assimilating shape and intensity with EnKF

In practice, we have more observations than just the positions of the hurricanes. The experiments in this

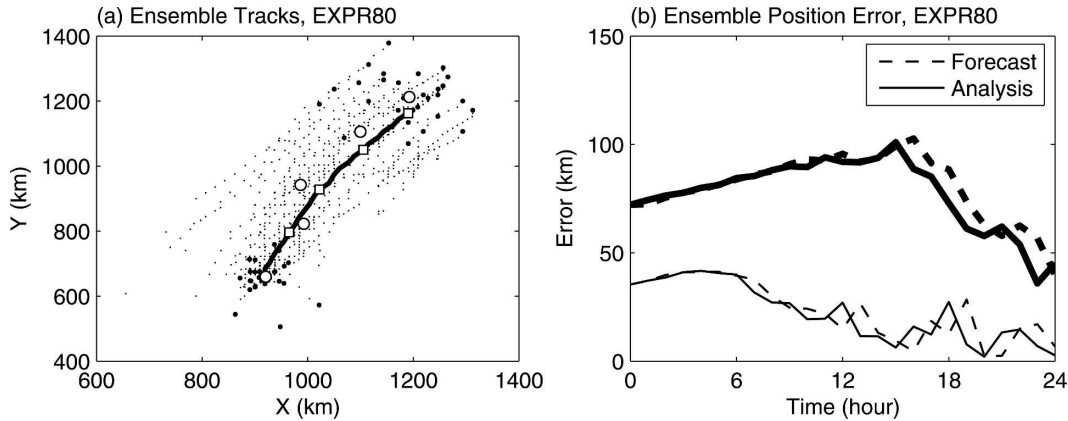


FIG. 6. Same as Fig. 5, but for experiment EXPR80 with initial track error of 80 km.

subsection test whether the assimilation of other information about the vortex, such as its shape and intensity, can partially counteract the breakdown of the EnKF for large displacements.

Experiment EXPR80S is the same as EXPR80 except three vortex-shape parameters (length of major and minor axes, rotation angle) are assimilated along with the center positions. The observations of the shape parameters are constructed as discussed in section 3b and have Gaussian errors of standard deviations of 20 km for the axes and 45° for the angle of the elliptic shape. To demonstrate the benefits of assimilating more observations, the same realization of the position observations as in EXPR80 is utilized in the subsequent experiments.

Figure 8 shows the ensemble tracks and errors for EXPR80S. The spread of the ensemble tracks quickly

decreases to about 11 km in just four assimilation cycles, and it stays steadily at that level thereafter. The ensemble tracks align nicely with the real track. The correlation diagnostic (Fig. 9) reveals that EXPR80S also captures the vortex structure much more faithfully. The correlations are higher than 0.8 and their mean is above 0.9 except in the first three cycles. The ensemble spreads for the major and minor axes are as large as 35 km in the first several assimilation cycles, then quickly reduce to a constant level of about 5 km. Assimilating the shape parameters thus not only encourages the ensemble tracks to converge rapidly toward the real track, but also helps the vortices in each member to maintain structures similar to the reference vortex.

We have also experimented with assimilating only the average length of the vortex's axes as a simple measure of vortex size, rather than all three scalar-shape

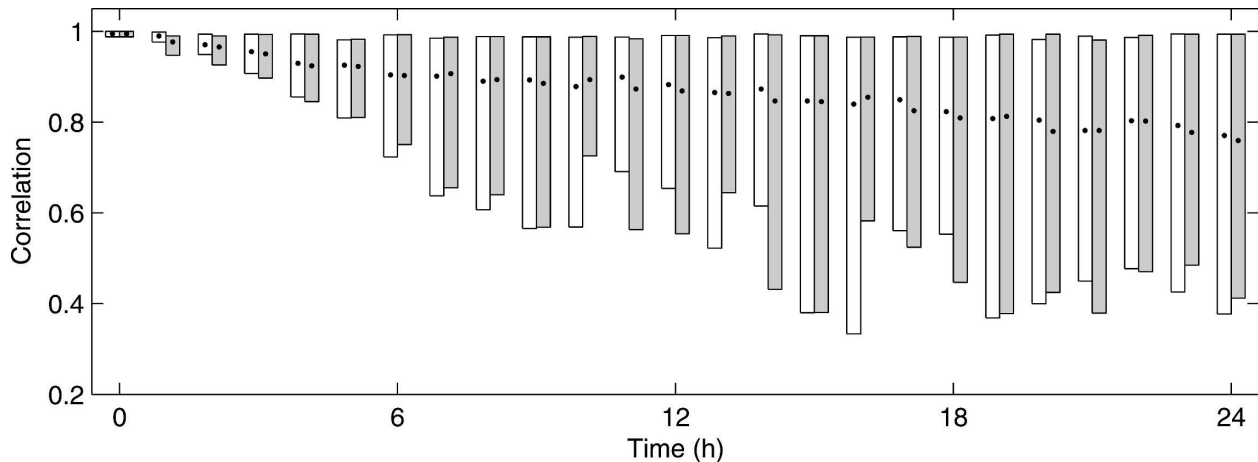


FIG. 7. Correlations of the vorticity fields around the vortex center between ensemble members and the reference simulation. The white and gray bars represent the range of the correlation values at the forecast steps and the analysis steps, respectively. The black dots inside the bars indicate the ensemble mean correlations.

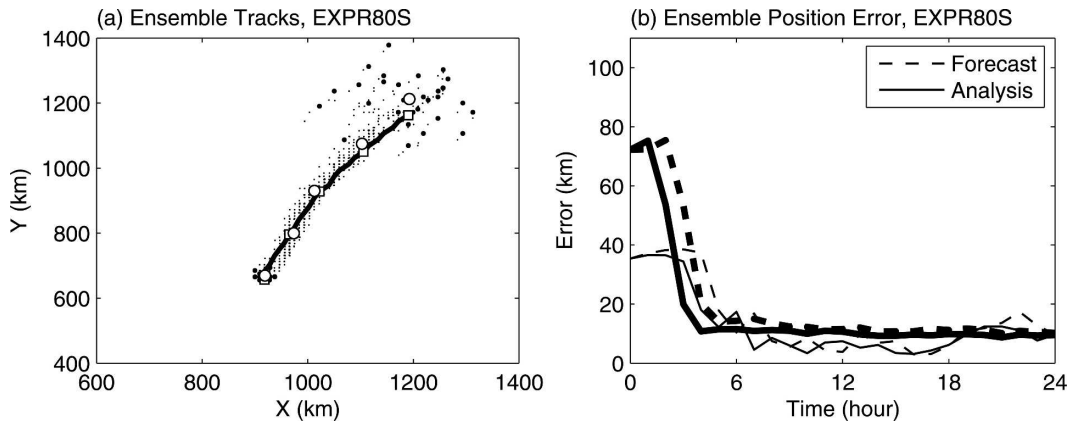


FIG. 8. Same as Fig. 6, but for experiment EXPR80S with the shape parameters assimilated.

parameters. In such tests (not shown), the size observations alone substantially reduce the ensemble track divergence, but the reduction occurs over 10 assimilation cycles rather than 4 as in EXPR80S and the correlation diagnostic remains significantly worse even after 24 cycles. Although assimilating only the vortex size has the virtue of simplicity, all three shape parameters thus appear useful in correcting the problems created by the position update in EXPR80.

Since the correlations are computed only in small regions around the vortex centers, some ensemble members with large center displacements may still contain significant vorticity anomalies near their initial centers during the first several hours. Interactions of these asymmetric anomalies with the main vortex could significantly affect its track (Chan and Williams 1987; Smith et al. 1990; Smith 1991) and intensity (Montgomery and Kallenbach 1997; Wang 2002; Chen et al. 2003; Chen and Yau 2003). The assimilations should continue

for some extra time period (on the order of vortex turnover time) to allow the main vortex to axisymmetrize the surrounding anomalies before any ensemble forecast is started. Alternatively, the asymmetric anomalies could be weakened by assimilating accurate intensity or some other observations.

The simple examples of section 3b suggested that intensity observations could also compensate for problems in the EnKF's assimilation of position. In a new experiment, EXPR80I, intensity observations instead of the shape parameters are assimilated. This experiment uses the same initial conditions and position observations as EXP80S. The intensity observations are taken from the reference vortex with Gaussian errors of mean zero and standard deviation of  $10^{-3} \text{ s}^{-1}$ . The convergence of the ensemble tracks toward the observed track is similar to that in EXP80S, but the correlations of the vortex structure with that of the true vortex do not recover to values above 0.8 until 12 h (not shown).

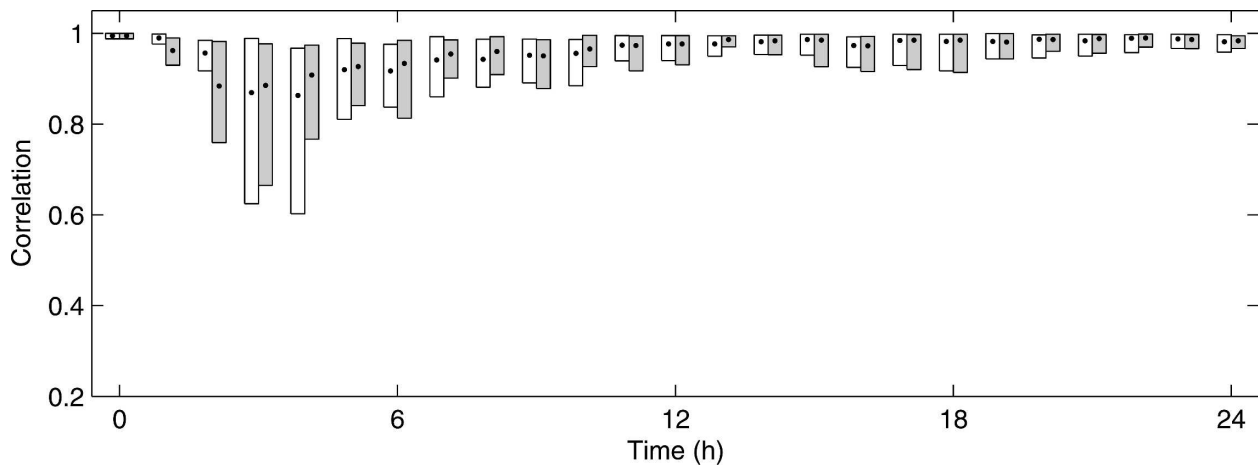


FIG. 9. Same as Fig. 7, but for experiment EXPR80S with the shape parameters assimilated.

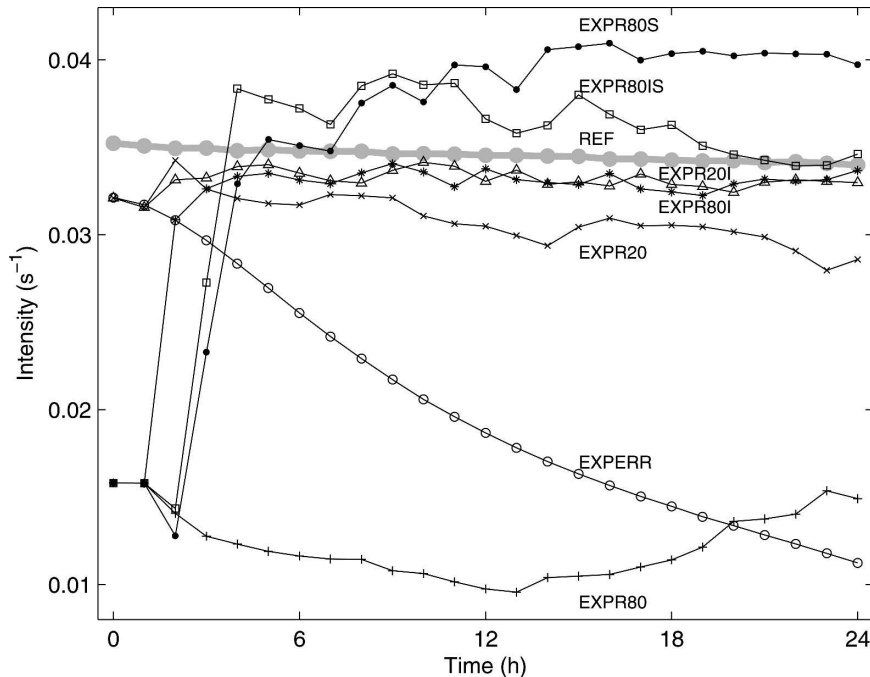


FIG. 10. Comparison of the intensities ( $s^{-1}$ ) of the ensemble mean vortices. The thick gray dotted line is the intensity of the reference vortex in experiment EXPR80.

It appears that the assimilation of intensity does not regulate the shape of the vortex as effectively and thus some ensemble members need a longer time to symmetrize.

The main advantage of assimilating accurate intensity observations is to match the intensities of the ensemble vortices to the reference vortex. Figure 10 compares the hourly intensities of the ensemble mean vortices at the forecast steps in several different experiments. The thick gray line with dots denotes the intensity of the reference vortex in EXPR80, which is very similar to the intensity of the reference vortex in EXPERR and EXPR20. Without data assimilation, the mean vortex becomes weaker and weaker with time because the inherent smoothing of the ensemble mean increases as the members' tracks diverge (EXPERR). Assimilating the center position can only substantially reduce this weakening by maintaining small displacements among the members (EXPR20), but it can fail for initially large displacements (EXPR80). The best analyses for the intensity, as might be expected, are obtained by assimilating accurate intensities (EXPR20I and EXPR80I). Here the experiment EXPR20I is very similar to EXPR20 except the intensity observations are assimilated along with the vortex center positions.

The low bias in the intensity of the mean vortex is a generic consequence of finite displacements, as can be seen by retaining the quadratic terms in (5) and com-

puting the mean. On the other hand, the analysis overestimates the intensity when only shape parameters are included with position observations in the assimilation (EXPR80S). This suggests that the analysis should be based on the assimilation of the shape, intensity, and center position of the vortex.

Observations of the intensity of a hurricane, however, may contain large errors, especially when the hurricane is far from land so that only satellite imagery is available for intensity estimation (Gray et al. 1991). In the next experiment, EXPR80IS, both the intensity and the shape parameters are assimilated and intensity observation errors are taken to have the relatively large standard deviation of  $10^{-2} s^{-1}$  to mimic reality. This experiment also uses the same initial conditions and the same observations of position and shape parameters as in EXPR80S. Similar to EXPR80S, the tracks quickly converge (Fig. 11d). The analysis is also able to bring back the overestimated intensity to a desirable value in 20 cycles (Fig. 10).

#### e. Improvement of track forecast

When the initial displacements of vortices are not too large, assimilating the position, shape, and intensity of a vortex with the EnKF for several vortex turnover times generates an ensemble analysis in which the vortices in all the ensemble members move at approximately the correct speed and track and develop structure consis-

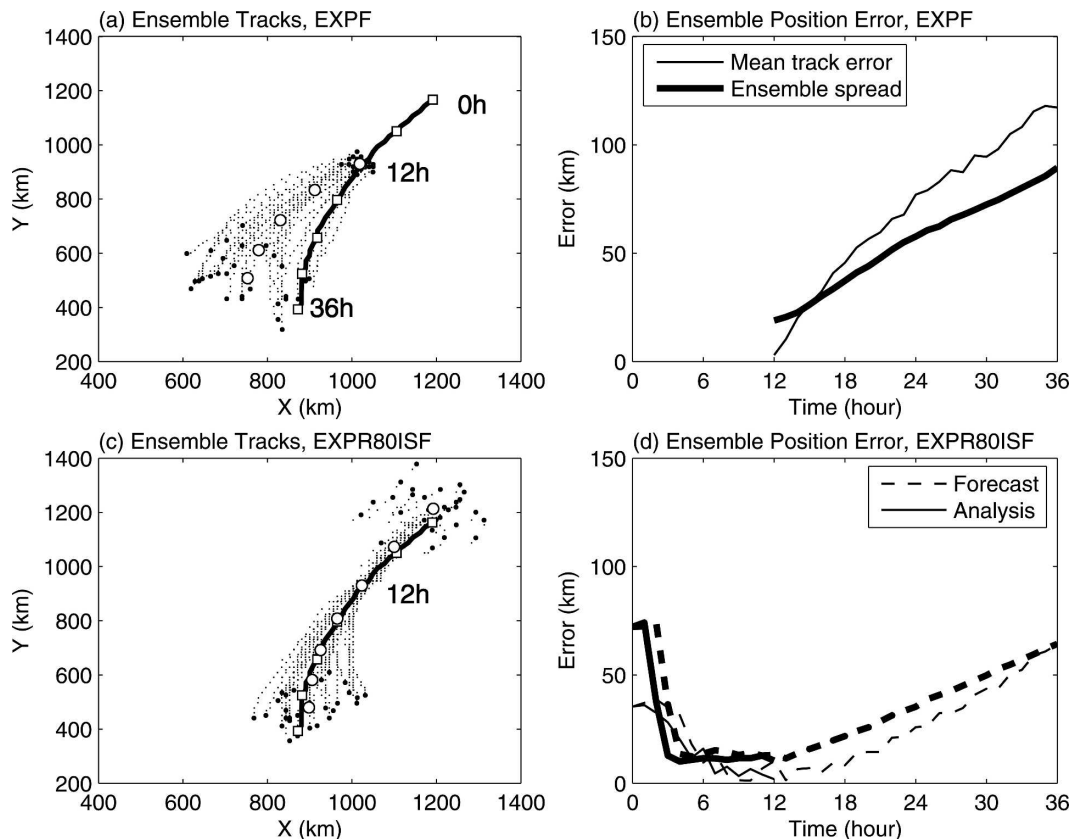


FIG. 11. Same as Fig. 5, but for experiment (a), (b) EXPF and (c), (d) EXPR80ISF.

tent with the observations. We next ask how forecasts from such analyses would compare to those based on a simple bogusing scheme that inserts a vortex (or ensemble of vortices) whose intensity and location are approximately correct.

Here we compare the 24-h forecasts in two experiments, EXPR80ISF and EXPF. Experiment EXPR80ISF is the same as EXPR80IS except there is no data assimilation after 12 h. Experiment EXPF is an ensemble forecast initialized similarly to EXPERR, which represents a simple vortex bogusing scheme. In EXPF, the vorticity field integrated without the vortex at 252 h is used as the large-scale environmental flow, which is then randomly perturbed. The reference vortex at 12 h in EXPR80IS is taken as the true vortex. The initial vortices to be bogused into the perturbed large-scale environmental flow have an axisymmetric Gaussian vorticity profile with the same maximum intensity as the true vortex and a decay scale of 80 km in the radial direction. Their center coordinates, however, are drawn randomly from a Gaussian distribution with mean equal to the center coordinates of the true vortex and a standard deviation of 20 km. Initially, the major and minor axes for the true vortex are 69 and 66 km,

respectively. The ensemble vortices in EXPF have similar mean axes of 68 and 67 km, respectively, while the values for EXPR80ISF are larger (79 and 72 km). In both experiments, the forecasts extend for an additional 24 h.

Figure 11 plots the ensemble tracks and their errors in the two forecast experiments. The ensemble tracks diverge without the assimilation in both experiments. In EXPR80ISF, all the ensemble members are confined in the vicinity of the true track and the ensemble mean track and the true track align well. The errors of the mean track and the ensemble spread increase from 2 and 11 km, respectively, at 12 h to about 64 km at 36 h. A deterministic forecast using only the ensemble mean at 12 h gives nearly the same results as the mean in this ensemble forecast. In contrast, the center positions of the ensemble vortices in EXPF are biased to the right of the track even though they are initialized centered around the true location. The error of the mean track increases rapidly from 3 km at 12 h to 117 km at 36 h, while the spread of positions increases from 19 to 89 km.

Inspection of the vorticity field (not shown) indicates that the true vortex is significantly influenced by its

interaction with the large anticyclone to its northwest (cf. Fig. 4). The vortex advects the negative vorticity southward and eastward. That change in large-scale vorticity (negative vorticity to the southwest of the vortex) is captured by the EnKF analysis but not by the bogusing technique in which a symmetric vortex is simply added to the large-scale flow. The flow in the EXPR80ISF analysis is then more northwesterly near the vortex, relative to that in EXPF, and the forecasts in EXPF are displaced to the northwest relative to EXPR80ISF.

This experiment in a simple model is certainly insufficient to conclude that the EnKF analysis will always produce better forecasts than an analysis using some form of vortex bogusing. A comparison of the two for real hurricane forecasts will be reported in the future.

## 5. Discussion and conclusions

Despite the advances in observation capabilities and data assimilation techniques, initializing a realistic vortex having the correct location and motion remains a challenge in hurricane forecast models. The existing vortex bogusing methods can generate a reasonable initial vortex, but the subsequent forecast may undergo vigorous adjustments and false spinup owing to the inconsistencies of the initial vortex and the initial conditions of the forecast model. This can result in poor forecasts of track or intensity. Four-dimensional variational methods have the potential to produce model-consistent initial vortices. Implementing the tangent linear and adjoint models for the variational methods, however, is not trivial, especially when the observations (such as position in this study) have highly nonlinear observation operators.

A new vortex initialization method, based on the EnKF, is proposed in this paper. Hurricane position and other characteristics, which can be estimated almost from satellite and radar imagery, can be easily assimilated with the EnKF. The same model, including full nonlinearity and full physics, is utilized for the analysis and the forecast. The spurious transient evolution of the initial vortex produced by other initialization schemes is reduced.

In the limit of small prior position error, the errors in physical fields have a distribution that is approximately Gaussian if the position error is Gaussian. The EnKF update is then close to optimal and smoothly shifts the prior vortices toward the observed center. When the initial position error is comparable to or larger than the vortex size, the errors in the physical field will not be Gaussian even in the case that the position error is. This results in poor performance of the EnKF. For example,

if a member's vortex is far from the observed center, the EnKF update will create an additional vortex near the observed center rather than shifting the original vortex.

Numerical experiments using a simple 2D barotropic model demonstrate that assimilating only position observations with an EnKF can prevent the divergence of vortex tracks that would occur without assimilation. When the initial position errors are small, the EnKF produces an analysis in which all the ensemble vortices are confined, within observational uncertainty, to the correct locations. However, the EnKF begins to fail when the position errors are significant compared to the size of the vortex, which may occur if the position observations are inaccurate or available infrequently. The EnKF update then produces highly asymmetric structures for some members' vortices and may even, as just noted, create additional vortices.

The effectiveness of the EnKF can be extended if vortex shape and/or intensity observations are assimilated along with the positions. The "shape" of a vortex is defined in this study by three parameters (namely, the major axis, the minor axis, and the rotation angle) that are retrieved from a best fit ellipse using the elliptic Fourier descriptor (EFD) method. By regulating the distorted vortex shape, the assimilation of the shape parameters after the position significantly reduces the ensemble spread of the vortex positions and leads to quicker convergence of the ensemble tracks. Similar improvement can be obtained if accurate intensity observations are assimilated. While assimilating shape parameters can help the vortices in each member to develop structure similar to the reference vortex, assimilating intensity observations maintains the correct vortex intensity. The assimilation of both the shape parameters and the intensity after the position produces the best analysis. We emphasize, however, that assimilating shape or intensity observations does not address in any fundamental way problems arising from the EnKF's linear update when the underlying distributions are non-Gaussian. Instead, those observations merely provide additional information that can partially compensate for pathologies in the EnKF analysis.

Within several vortex turnover times, the assimilation as well as the vortex internal dynamics force the ensemble vortices to develop structures and intensities consistent with the observations and to move along the correct track. The subsequent ensemble or deterministic forecasts in the barotropic example are improved.

Based on its success in the simple 2D framework, we plan to apply this technique to real hurricane cases using a more sophisticated mesoscale model (e.g., Weather Research and Forecast model). There are, of

course, a variety of other observations relevant for the analysis and forecasting of hurricanes. The assimilation of vortex position should enhance the use of these other observations by ensuring that the prior forecast used in the assimilation has the hurricane in the correct location.

*Acknowledgments.* The authors thank Drs. Alain Caya and Qingnong Xiao for their helpful discussion. Dr. Greg Lawson and an anonymous reviewer made many helpful comments that led to improvements of the manuscript. This research was supported at NCAR by NSF Grant 0205655. The first author is also sponsored by the Natural Sciences and Engineering Research Council of Canada and the Canadian Space Agency.

## APPENDIX

### Elliptic Fourier Descriptor

The elliptic Fourier descriptor is widely used in image processing and pattern recognition. In the EFD method, a closed and chain-encoded contour is represented by a Fourier series in terms of the segment length of an arbitrary point from a starting point of the contour. If the linear segment between the two adjacent ( $i - 1$  and  $i$ th) points is  $\Delta t_i$ , the length of the contour from the starting point to the  $p$ th point is  $t_p = \sum_{i=1}^p \Delta t_i$  and the perimeter of the contour is  $T = t_K$ , where  $K$  is the total number of the points on the contour. Correspondingly, the  $x$  coordinate of the  $p$ th point is  $x_p = \sum_{i=1}^p \Delta x_i$ , where  $\Delta x_i$  is the displacement along the  $x$  axis of the contour between the  $i - 1$  and  $i$ th points. The elliptic Fourier series expansion for the  $x$  coordinates up to  $N$  harmonics is

$$x_p = A_0 + \sum_{n=1}^N \left( a_n \cos \frac{2n\pi t_p}{T} + b_n \sin \frac{2n\pi t_p}{T} \right), \quad (\text{A1})$$

where

$$a_n = \frac{T}{2n^2\pi^2} \sum_{p=1}^K \frac{\Delta x_p}{\Delta t_p} \left( \cos \frac{2n\pi t_p}{T} - \cos \frac{2n\pi t_{p-1}}{T} \right), \quad (\text{A2})$$

and

$$b_n = \frac{T}{2n^2\pi^2} \sum_{p=1}^K \frac{\Delta x_p}{\Delta t_p} \left( \sin \frac{2n\pi t_p}{T} - \sin \frac{2n\pi t_{p-1}}{T} \right). \quad (\text{A3})$$

Corresponding coefficients  $c_n$  and  $d_n$  for the  $y$  coordinate are computed in the same manner. Only coefficients for  $n = 1$  are computed in this paper. Using four coefficients ( $a_1$ ,  $b_1$ ,  $c_1$ , and  $d_1$ ) and the properties of an ellipse, the major and minor axes and the rotation angle can be obtained. Interested readers can find a comprehensive description of EFD from Kuhl and Giardina (1982).

Strictly speaking, the ellipse is not exactly the symmetric component plus the wavenumber two asymmetry w.r.t the vortex center. The ellipse determined by the EFD method may not be centered at the vorticity-weighted center of the vortex, since uniform density is assumed when calculating the center point ( $A_0$ ,  $C_0$ ) in EFD.

## REFERENCES

- Aberson, S. D., and M. DeMaria, 1994: Verification of a nested barotropic hurricane track forecast model (VICBAR). *Mon. Wea. Rev.*, **122**, 2804–2815.
- , M. A. Bender, and R. E. Tuleya, 1998: Ensemble forecasting of tropical cyclone tracks. Preprints, *12th Conf. on Numerical Weather Prediction*, Phoenix, AZ, Amer. Meteor. Soc., 290–292.
- Anderson, J. L., B. Wyman, S. Zhang, and T. Hoar, 2005: Assimilation of surface pressure observations using an ensemble filter in an idealized global atmospheric prediction system. *J. Atmos. Sci.*, **62**, 2925–2938.
- Bender, M. A., R. J. Ross, R. E. Tuleya, and Y. Kurihara, 1993: Improvements in tropical cyclone track and intensity forecasts using the GFDL initialization system. *Mon. Wea. Rev.*, **121**, 2046–2061.
- Burpee, R. W., S. D. Aberson, J. L. Franklin, S. J. Lord, and R. E. Tuleya, 1996: The impact of Omega dropwindsondes on operational hurricane track forecast models. *Bull. Amer. Meteor. Soc.*, **77**, 925–933.
- Carr, L. E., III, and R. T. Williams, 1989: Barotropic vortex stability to perturbations from axisymmetry. *J. Atmos. Sci.*, **46**, 3177–3191.
- Chan, J. C., and R. T. Williams, 1987: Analytical and numerical studies of the beta-effect in tropical cyclone motion. Part I: Zero mean flow. *J. Atmos. Sci.*, **44**, 1257–1265.
- Chen, Y., and M. K. Yau, 2003: Asymmetric structures in a simulated landfalling hurricane. *J. Atmos. Sci.*, **60**, 2294–2312.
- , G. Brunet, and M. K. Yau, 2003: Spiral bands in a simulated hurricane. Part II: Wave activity diagnostics. *J. Atmos. Sci.*, **60**, 1239–1256.
- Cheung, K. K. W., and J. C. L. Chan, 1999a: Ensemble forecasting of tropical cyclone motion using a barotropic model. Part I: Perturbations of the environment. *Mon. Wea. Rev.*, **127**, 1229–1243.
- , and —, 1999b: Ensemble forecasting of tropical cyclone motion using a barotropic model. Part II: Perturbations of the vortex. *Mon. Wea. Rev.*, **127**, 2617–2640.
- Davidson, N. E., and H. C. Weber, 2000: The BMRC high-resolution tropical cyclone prediction system: TC-LAPS. *Mon. Wea. Rev.*, **128**, 1245–1265.
- DeMaria, M., S. D. Aberson, K. V. Ooyama, and S. J. Lord, 1992:

- A nested spectral model for hurricane track forecasting. *Mon. Wea. Rev.*, **120**, 1628–1643.
- Dowell, D. C., F. Zhang, L. J. Wicker, C. Snyder, and N. A. Crook, 2004: Wind and thermodynamic retrievals in the 17 May 1981 Arcadia, Oklahoma, supercell: Ensemble Kalman filter experiments. *Mon. Wea. Rev.*, **132**, 1982–2005.
- Dvorak, V. F., 1975: Tropical cyclone intensity analysis and forecasting from satellite imagery. *Mon. Wea. Rev.*, **103**, 420–430.
- , 1984: Tropical cyclone intensity analysis using satellite data. NOAA Tech. Rep. NESDIS 11, 47 pp.
- Elsberry, R., 1995: Tropical cyclone motion. *Global Perspective on Tropical Cyclones*, WMO/TD 693, R. Elsberry, Ed., WMO, 160–197.
- Evensen, G., 1994: Sequential data assimilation with a nonlinear quasi-geostrophic model using Monte Carlo methods to forecast error statistics. *J. Geophys. Res.*, **99**, 10 143–10 162.
- , 2003: The ensemble Kalman filter: Theoretical formulation and practical implementation. *Ocean Dyn.*, **53**, 343–367.
- Franklin, J. L., C. J. McAdie, and M. B. Lawrence, 2003: Trends in track forecasting for tropical cyclones threatening the United States, 1970–2001. *Bull. Amer. Meteor. Soc.*, **84**, 1197–1203.
- Gray, W. M., C. Neumann, and T. L. Tsui, 1991: Assessment of the role of aircraft reconnaissance on tropical cyclone analysis and forecasting. *Bull. Amer. Meteor. Soc.*, **72**, 1867–1883.
- Hamill, T. M., and C. Snyder, 2000: A hybrid ensemble Kalman filter–3D variational analysis scheme. *Mon. Wea. Rev.*, **128**, 2905–2919.
- Heming, J. T., S. Robinson, C. Woolcock, and K. Mylne, 2004: Tropical cyclone ensemble forecast product development and verification at the Met Office. Preprints, *26th Conf. on Hurricanes and Tropical Meteorology*, Miami, FL, Amer. Meteor. Soc., 158–159.
- Hoffman, B. N., Z. Liu, J.-F. Louis, and C. Grassotti, 1995: Distortion representation of forecast errors. *Mon. Wea. Rev.*, **123**, 2758–2770.
- Houtekamer, P. L., and H. L. Mitchell, 1998: Data assimilation using an ensemble Kalman filter technique. *Mon. Wea. Rev.*, **126**, 796–811.
- , —, G. Pellerin, M. Buehner, M. Charron, L. Spacek, and B. Hansen, 2005: Atmospheric data assimilation with an ensemble Kalman filter: Results with real observations. *Mon. Wea. Rev.*, **133**, 604–620.
- Kalman, R. E., 1960: A new approach to linear filtering and prediction problems. *J. Basic Eng.*, **82D**, 35–45.
- , and R. S. Bucy, 1961: New results in linear filtering and prediction theory. *J. Basic Eng.*, **83D**, 95–108.
- Krishnamurti, T. N., R. Correa-Torres, G. Rohaly, and D. Oosterhof, 1997: Physical initialization and hurricane ensemble forecasts. *Wea. Forecasting*, **12**, 503–514.
- Kuhl, F. P., and C. R. Giardino, 1982: Elliptic Fourier features of a closed contour. *Comput. Graphics Image Process.*, **18**, 236–258.
- Kurihara, Y., M. A. Bender, and R. J. Ross, 1993: An initialization scheme of hurricane models by vortex specification. *Mon. Wea. Rev.*, **121**, 2030–2045.
- , R. E. Tuleya, and M. A. Bender, 1998: The GFDL hurricane prediction system and its performance in the 1995 hurricane season. *Mon. Wea. Rev.*, **126**, 1306–1322.
- Lawson, G. W., and J. A. Hansen, 2005: Alignment error models and ensemble-based data assimilation. *Mon. Wea. Rev.*, **133**, 1687–1709.
- Leidner, S. M., L. Isaksen, and R. N. Hoffman, 2003: Impact of NSCAT winds on tropical cyclones in the ECMWF 4DVAR assimilation system. *Mon. Wea. Rev.*, **131**, 3–26.
- Leslie, L. M., and G. J. Holland, 1995: On the bogussing of tropical cyclones in numerical models: A comparison of vortex profiles. *Meteor. Atmos. Phys.*, **56**, 101–110.
- Liu, Q., T. Marchok, H.-L. Pan, M. Bender, and S. Lord, 2002: Improvements in hurricane initialization and forecasting at NCEP with global and regional (GFDL) models. Tech. Procedures Bull. 472, NCEP/EMC Tech. Rep., 7 pp.
- Liu, Y., D.-L. Zhang, and M. K. Yau, 1997: A multiscale numerical study of Hurricane Andrew (1992). Part I: Explicit simulation and verification. *Mon. Wea. Rev.*, **125**, 3073–3093.
- Lord, S. J., 1991: A bogusing system for vortex circulations in the National Meteorological Center global forecast model. Preprints, *19th Conf. on Hurricanes and Tropical Meteorology*, Miami, FL, Amer. Meteor. Soc., 328–330.
- Marchok, T. P., Z. Toth, and Q. Liu, 2002: Use of the NCEP global ensemble for tropical cyclone track forecasting. Preprints, *25th Conf. on Hurricanes and Tropical Meteorology*, San Diego, CA, Amer. Meteor. Soc., 176–177.
- Melander, M. V., J. C. McWilliams, and N. J. Zabusky, 1987: Axisymmetrization and vorticity-gradient intensification of an isolated two-dimensional vortex through filamentation. *J. Fluid Mech.*, **178**, 137–159.
- Mitchell, H. L., P. L. Houtekamer, and G. Pellerin, 2002: Ensemble size, balance, and model-error representation in an ensemble Kalman filter. *Mon. Wea. Rev.*, **130**, 2791–2808.
- Montgomery, M. T., and R. J. Kallenbach, 1997: A theory for vortex Rossby-waves and its application to spiral bands and intensity changes in hurricanes. *Quart. J. Roy. Meteor. Soc.*, **123**, 435–465.
- Morss, R. E., K. A. Emanuel, and C. Snyder, 2001: Idealized adaptive observation strategies for improving numerical weather prediction. *J. Atmos. Sci.*, **58**, 210–232.
- Pu, Z., and S. A. Braun, 2001: Evaluation of bogus vortex techniques with four-dimensional variational data assimilation. *Mon. Wea. Rev.*, **129**, 2023–2039.
- Ravela, S., K. Emanuel, and D. McLaughlin, 2004: Data assimilation by field alignment for coherent structures. Preprints, *26th Conf. on Hurricanes and Tropical Meteorology*, Miami, FL, Amer. Meteor. Soc., 560–561.
- Serrano, E., and P. Undén, 1994: Evaluation of a tropical cyclone bogusing method in data assimilation and forecasting. *Mon. Wea. Rev.*, **122**, 1523–1547.
- Smith, G. B., and M. T. Montgomery, 1995: Vortex axisymmetrization: Dependence on azimuthal wavenumber or asymmetric radial structure changes. *Quart. J. Roy. Meteor. Soc.*, **121**, 1615–1650.
- Smith, R. K., 1991: An analytic theory of tropical-cyclone motion in a barotropic shear flow. *Quart. J. Roy. Meteor. Soc.*, **117**, 685–714.
- , W. Ulrich, and G. Dietachmayer, 1990: A numerical study of tropical cyclone motion using a barotropic model. Part I: The role of vortex asymmetries. *Quart. J. Roy. Meteor. Soc.*, **116**, 337–362.
- Snyder, C., and F. Zhang, 2003: Assimilation of simulated Doppler radar observations with an ensemble Kalman filter. *Mon. Wea. Rev.*, **131**, 1663–1677.
- Sutyrin, G. G., 1989: Azimuthal waves and symmetrization of an intense vortex. *Sov. Phys. Dokl.*, **34**, 104–106.
- Vigh, J., 2004: Evaluation of a kilo-member ensemble for track forecasting. Preprints, *26th Conf. on Hurricanes and Tropical Meteorology*, Miami, FL, Amer. Meteor. Soc., 160–161.

- Wang, Y., 2002: Vortex Rossby waves in a numerically simulated tropical cyclone. Part II: The role in tropical cyclone structure and intensity change. *J. Atmos. Sci.*, **59**, 1239–1262.
- Weber, H., 2003: Hurricane track prediction using a statistical ensemble of numerical models. *Mon. Wea. Rev.*, **131**, 749–770.
- Whitaker, J., and T. M. Hamill, 2002: Ensemble data assimilation without perturbed observations. *Mon. Wea. Rev.*, **130**, 1913–1924.
- Xiao, Q., X. Zou, and B. Wang, 2000: Initialization and simulation of a landfalling hurricane using a variational bogus data assimilation scheme. *Mon. Wea. Rev.*, **128**, 2252–2269.
- Zhang, F., C. Snyder, and J. Sun, 2004: Impacts of initial estimate and observation availability on convective-scale data assimilation with an ensemble Kalman filter. *Mon. Wea. Rev.*, **132**, 1238–1253.
- Zhang, Z., and T. N. Krishnamurti, 1997: Ensemble forecasting of hurricane tracks. *Bull. Amer. Meteor. Soc.*, **78**, 2785–2795.
- , and —, 1999: A perturbation method for hurricane ensemble predictions. *Mon. Wea. Rev.*, **127**, 447–469.
- Zhu, T., D.-L. Zhang, and F. Weng, 2002: Impact of the Advanced Microwave Sounding Unit measurements on hurricane prediction. *Mon. Wea. Rev.*, **130**, 2416–2432.
- Zou, X., and Q. Xiao, 2000: Studies on the initialization and simulation of a mature hurricane using a variational bogus data assimilation scheme. *J. Atmos. Sci.*, **57**, 836–860.